VPS VIBRATIONS IN PHYSICAL SYSTEMS

DOI: 10.21008/j.0860-6897.2023.2.05
Vibrations in Physical Systems, 2023, 34(2), 2023205

The effect of evanescent modes on low-frequency sound field in rectangular rooms

Mirosław MEISSNER

Institute of Fundamental Technological Research, Polish Academy of Sciences, Pawińskiego 5B, 02-106 Warsaw

Corresponding author: Mirosław MEISSNER, email: mmeissn@ippt.pan.pl

Abstract The paper investigates the sound field excited by a boundary pure-tone source in rigid-walled rectangular rooms. This approach is applicable in the low-frequency range, where sound absorption by wall surfaces can be considered negligible. The sound pressure was theoretically determined by applying the Green's function based on the cut-on and evanescent modes expansion instead of the usual normal mode expansion. The theoretical model was used to predict the spatial distribution of the sound pressure level at different source frequencies. The calculation results have shown that for audible frequencies below the cut-off frequency, the plane wave mode and evanescent modes strongly interfere which results in an interference pattern with large dips in the pressure level forming a continuous curve. A shape of this curve is highly dependent on the excitation frequency. These dips have been found to occur when the sound associated with the plane wave mode is cancelled by the sound produced by evanescent modes.

Keywords: rectangular room, evanescent modes, plane wave mode, sound cancellation, sound intensity.

1. Introduction

The excitation of evanescent modes must be considered in the analysis of acoustic wave propagation whenever radiation, reflection, transmission or diffraction of sound waves is investigated. A characteristic feature of evanescent modes is that they do not propagate, but decay exponentially in a certain spatial direction. A classical problem presented in acoustics textbooks is a sound field produced by a time-harmonic source placed inside the acoustic waveguide, because in this case the field can be decomposed into a sum of a finite number of propagating modes and an infinite number of evanescent modes [1,2].

A number of studies conducted in the past have focused on the excitation of evanescent modes in the cavity resonators, resulting in an aperture length correction that modifies the resonant frequency [3,4]. The influence of evanescent modes on the natural frequencies was also studied in the system consisting of multiple rectangular cavities connected by necks or slits in series [5]. Evanescent modes are also excited in rectangular rooms, but the research effort has been directed to the theoretical and numerical analysis of the sound field in reverberant and steady-state conditions [6,7], as well as at determining the optimum dimension ratios for small rectangular rooms in order to obtain a smoother frequency response at low frequencies [8]. In these studies, the indoor sound field was modelled using the normal mode expansion, therefore the influence of evanescent modes on this field was not examined.

The paper is organized as follows. Following the Introduction, Sect. 2 presents a theoretical model of a sound field inside rectangular rooms based on the cut-on and evanescent modes expansion. Section 3 discusses the results of numerical study. The paper is concluded with final remarks in Sect. 4.

2. Theoretical analysis

The most convenient way to describe the sound field inside enclosed spaces is to use the Green's function $G(\mathbf{r}|\mathbf{r}_s)$ describing the pressure response at the receiving point $\mathbf{r} = (x, y, z)$ to the sound excitation at the source point $\mathbf{r}_s = (x_s, y_s, z_s)$. The Green's function is very useful in room acoustics because knowing its form allows to predict the room response to any sound source. If the indoor sound field is produced by the boundary source having a time-harmonic behavior $e^{\mathrm{j}\omega t}$ with a radial frequency ω, the pressure response to this excitation can be determined from the following equation (the factor $e^{\mathrm{j}\omega t}$ was excluded)

$$p(\mathbf{r}) = -\mathrm{j}\rho ck \iint_{S_w} u(\mathbf{r}_s) G(\mathbf{r}|\mathbf{r}_s)\, \mathrm{d}S_w, \tag{1}$$

where ρ and c are the air density and sound speed inside the room, $k = \omega/c$ is the wave number, $u(\mathbf{r}_s)$ is the normal velocity on the room walls (positive outward), S_w is the wall surface and $\mathrm{j} = \sqrt{-1}$.

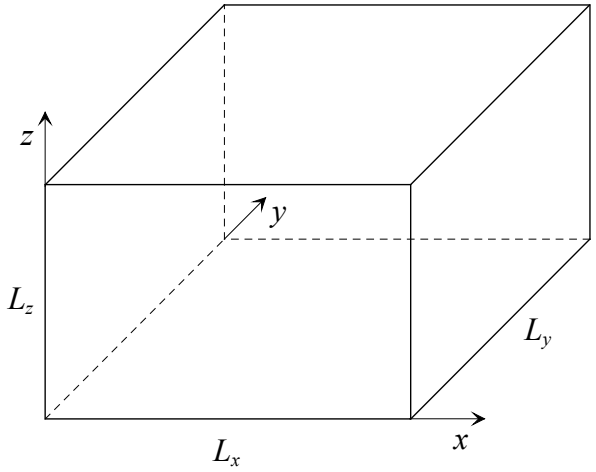

Figure 1. A rectangular room under study together with the associated coordinate system.

A considered rectangular room together with the associated coordinate system is shown in Fig. 1. Since the theoretical analysis concerns the low-frequency sound range, it is assumed that the room walls are perfectly rigid, because in this frequency range soundproofing materials have negligible sound absorption [9]. In this case the Green's function $G(\mathbf{r}|\mathbf{r}_s)$ can be constructed as an infinite double series

$$G(\mathbf{r}|\mathbf{r}_s) = \sum_{m,n} \chi_{mn}(x|x_s)\psi_{mn}(y,z|y_s,z_s), \tag{2}$$

where the functions χ_{mn} and ψ_{mn} satisfy the following boundary conditions

$$\frac{\partial \chi_{mn}}{\partial x}(x=0) = \frac{\partial \chi_{mn}}{\partial x}(x=L_x) = 0, \tag{3}$$

$$\frac{\partial \psi_{mn}}{\partial y}(y=0) = \frac{\partial \psi_{mn}}{\partial y}\left(y=L_y\right) = \frac{\partial \psi_{mn}}{\partial z}(z=0) = \frac{\partial \psi_{mn}}{\partial z}(z=L_z) = 0, \tag{4}$$

and $m, n = 0,1,2 \ldots$ According to Ref. [1], the function ψ_{mn} meeting the boundary conditions (4) is given by

$$\psi_{mn}(y,z|y_s,z_s) = \frac{\mathrm{j}\epsilon_m\epsilon_n}{2k_{mn}L_yL_z}\cos\left(\frac{m\pi y}{L_y}\right)\cos\left(\frac{n\pi z}{L_z}\right)\cos\left(\frac{m\pi y_s}{L_y}\right)\cos\left(\frac{n\pi z_s}{L_z}\right), \tag{5}$$

where ϵ_m, ϵ_n are Neumann factors ($\epsilon_i = 1$ when $i = 0$, $\epsilon_i = 2$ when $i > 0$) and k_{mn} is determined by

$$k_{mn} = \sqrt{k^2 - \vartheta_{mn}^2}, \quad \vartheta_{mn} = \sqrt{\left(\frac{m\pi y}{L_y}\right)^2 + \left(\frac{n\pi z}{L_z}\right)^2}. \tag{6}$$

The procedure for finding the function χ_{mn} is as follows. Assume that a point sound source is located inside an infinitely long duct of rectangular cross-section $L_y \times L_z$. In this case the Green's function is determined by the following equation [1]

$$g(\mathbf{r}|\mathbf{r}_s) = \sum_{m,n} e^{\mathrm{j}k_{mn}|x-x_s|}\,\psi_{mn}(y,z|y_s,z_s). \tag{7}$$

Equation (7) shows, that in the low-frequency range, the source excites a finite number of modes that propagate ($k > \vartheta_{mn}$) and an infinite number of modes that are evanescent ($k < \vartheta_{mn}$), since these modes decay exponentially with increasing distance from the source. The Green's function $G(\mathbf{r}|\mathbf{r}_s)$ satisfying the boundary condition (3) can be determined by separating an area of length L_x from the duct ($0 \le x \le L_x$) and bounding it on both sides by perfectly rigid surfaces which are perpendicular to the duct walls. If there is a sound source located at point $\mathbf{r}_s = (x_s, y_s, z_s)$ in this area, the Green's function $G(\mathbf{r}|\mathbf{r}_s)$ will have

the form of an infinite series whose components represent successive reflections from both surfaces of the wave emitted by the source, i.e.

$$G(\mathbf{r}|\mathbf{r}_s) = \sum_{m,n} \psi_{mn} \left(e^{\mathrm{j}k_{mn}|x-x_s|} + e^{\mathrm{j}k_{mn}|x+x_s|} + \sum_{\mu=1}^{\infty} e^{\mathrm{j}k_{mn}|x-x_s-2\mu L_x|} + e^{\mathrm{j}k_{mn}|x-x_s+2\mu L_x|} + e^{\mathrm{j}k_{mn}|x+x_s-2\mu L_x|} + e^{\mathrm{j}k_{mn}|x+x_s+2\mu L_x|} \right) = \sum_{m,n} \psi_{mn} \left[e^{\mathrm{j}k_{mn}|x-x_s|} + e^{\mathrm{j}k_{mn}|x+x_s|} + 4\cos(k_{mn}x)\cos(k_{mn}x_s) \sum_{\mu=1}^{\infty} e^{2\mathrm{j}k_{mn}\mu L_x} \right]. \tag{8}$$

Considering that in Eq. (8) the infinite series in the square brackets may be replaced by the formula [10]

$$\sum_{\mu=1}^{\infty} e^{2\mathrm{j}k_{mn}\mu L_x} = \frac{\mathrm{j}\cot(k_{mn}L_x) - 1}{2}, \tag{9}$$

the following expression for the Green's function $G(\mathbf{r}|\mathbf{r}_s)$ can be found

$$G(\mathbf{r}|\mathbf{r}_s) = 2\mathrm{j} \sum_{m,n} \frac{\psi_{mn}(y,z|y_s,z_s)}{\sin(k_{mn}L_x)} \begin{cases} \cos(k_{mn}x_s)\cos[k_{mn}(L_x - x)], & x > x_s, \\ \cos(k_{mn}x)\cos[k_{mn}(L_x - x_s)], & x < x_s. \end{cases} \tag{10}$$

Now assume that $x_s = 0$ in Eq. (10), then after substituting Eqs. (5) and (10) into Eq. (1), the equation for the sound pressure, valid for $x > 0$, is obtained

$$p(\mathbf{r}) = \frac{\mathrm{j}\rho c \cos[k(L_x - x)]}{L_y L_z \sin(kL_x)} \iint_{S_w} u(\mathbf{r}_s)\,\mathrm{d}S_w + \frac{\mathrm{j}\rho ck}{L_y L_z} \left\{ \sum_{m,n} \frac{\mu_{mn}\cos[k_{mn}(L_x - x)]}{k_{mn}\sin(k_{mn}L_x)} - \sum_{m,n} \frac{\nu_{mn}\cosh[\beta_{mn}(L_x - x)]}{\beta_{mn}\sinh(\beta_{mn}L_x)} \right\} \cos\left(\frac{n\pi y}{L_y}\right)\cos\left(\frac{n\pi z}{L_z}\right) \times \iint_{S_w} u(\mathbf{r}_s)\cos\left(\frac{m\pi y_s}{L_y}\right)\cos\left(\frac{n\pi z_s}{L_z}\right)\mathrm{d}S_w, \tag{11}$$

where $\beta_{mn} = \sqrt{\vartheta_{mn}^2 - k^2}$ and $\mu_{mn} = 0$ for $m, n = 0$ and values of m, n for which $k < \vartheta_{mn}$, and $\mu_{mn} = \epsilon_m \epsilon_n$ for other m, n, and then, $\nu_{mn} = 0$ for values of m, n for which $k > \vartheta_{mn}$, and $\nu_{mn} = \epsilon_m \epsilon_n$ for other m, n. The first term in Eq. (11) describes the contribution of a plane wave to the sound field, while the other two terms describe the influence of propagating modes (so-called cut-on modes) and evanescent modes (so-called cut-off modes) on this field. The case where the boundary excitation takes the form of a source point is of particular importance from a theoretical point of view, because in such a situation the sound field is not affected by the shape and size of the source. If it is assumed that a source is located at the point $\mathbf{r}_0 = (0, y_0, z_0)$, then $u(\mathbf{r}_s) = u_a \delta(\mathbf{r}_s - \mathbf{r}_0)$, thus, in this case Eq. (11) takes the form

$$p(\mathbf{r}) = \frac{\mathrm{j}\rho cU \cos[k(L_x - x)]}{L_y L_z \sin(kL_x)} + \frac{\mathrm{j}\rho ckU}{L_y L_z} \left\{ \sum_{m,n} \frac{\mu_{mn}\cos[k_{mn}(L_x - x)]}{k_{mn}\sin(k_{mn}L_x)} - \sum_{m,n} \frac{\nu_{mn}\cosh[\beta_{mn}(L_x - x)]}{\beta_{mn}\sinh(\beta_{mn}L_x)} \right\} \cos\left(\frac{n\pi y}{L_y}\right)\cos\left(\frac{n\pi z}{L_z}\right)\cos\left(\frac{m\pi y_0}{L_y}\right)\cos\left(\frac{n\pi z_0}{L_z}\right), \tag{12}$$

where $U = Au_a$ is the volume velocity and $A = 1\ \mathrm{m}^2$ is the unit area. The following expression

$$\mathbf{u}(\mathbf{r}) = -\frac{1}{\mathrm{j}\rho\omega}\boldsymbol{\nabla} p(\mathbf{r}), \tag{13}$$

allows to determine a distribution of the velocity vector field in a room, where $\boldsymbol{\nabla}$ is the vector gradient operator $\boldsymbol{\nabla} = \mathbf{i}\,\partial/\partial \mathrm{x} + \mathbf{j}\,\partial/\partial \mathrm{y} + \mathbf{k}\,\partial/\partial \mathrm{z}$ and $\mathbf{i}$, $\mathbf{j}$, $\mathbf{k}$ are the versors in the rectangular coordinate system. In

terms of the pressure $p(\mathbf{r})$ and the velocity $\mathbf{u}(\mathbf{r})$, the complex sound intensity vector $\mathbf{I}_c$ describing the acoustic energy flux in a time-harmonic sound field can be determined using the well-known formula

$$\mathbf{I}_c(\mathbf{r}) = \frac{1}{2} p(\mathbf{r})\mathbf{u}^*(\mathbf{r}) = \mathbf{I}(\mathbf{r}) + \mathrm{j}\mathbf{Q}(\mathbf{r}), \tag{14}$$

where an asterisk in the superscript indicates the complex conjugate, $\mathbf{I}$ is called the active sound intensity or the acoustic intensity and $\mathbf{Q}$ is termed as the reactive sound intensity. The active component of the sound intensity describes the flow of acoustic energy in the sound field, while the reactive sound intensity represents the non-propagating, oscillatory sound energy flux. As follows from Eqs. (12) and (13), in the analyzed case the sound intensity $\mathbf{I}_c$ is represented only by the imaginary component. This is consistent with the results of previous studies [11] showing that for non-absorbent room walls, there is only oscillatory sound energy flow inside a room space.

3. Numerical study

As part of a numerical study, the sound pressure level was computed from the formula

$$\mathrm{SPL} = 20\log[P(\mathbf{r})/p_{\mathrm{ref}}], \tag{15}$$

where $P(\mathbf{r})$ is the pressure amplitude determined from Eq. (12) and $p_{\mathrm{ref}} = 2 \cdot 10^{-5}$ Pa. Calculations were run for the following room dimensions: $L_x = 4$ m, $L_y = 5$ m and $L_z = 3$ m. It was assumed that an air filling the room interior is characterized by the density $\rho = 1.21$ kg/m^3 and the speed of sound $c = 343$ m/s, thus, the cut-off frequency $f_c = c/2L_y$ is equal to 34.3 Hz. The room was excited by the boundary source located at the point: $x_0 = 0$ m, $y_0 = 2.5$ m and $z_0 = 1$ m. Such location of the point source enables to obtain a symmetrical distribution of sound field relative to the plane $y = 2.5$ m, which facilitates the interpretation of calculation results. The SPL was determined on the observation plane $z = 1.6$ m for the volume velocity U of 0.01 m^3/s. The first 1000 modes were used in the calculations.

As can be seen from Eq. (12), when the sound frequency f is much smaller than the cut-off frequency f_c, the formula for the pressure amplitude simplifies to the form

$$P \cong \frac{\rho c^2 U}{2\pi f V}, \tag{16}$$

where V is the room volume, so the pressure amplitude is the same at any point in the room. Moreover, P decreases inversely with frequency, thus, it has a very large value when the frequency tends to zero. This phenomenon is known as an excitation of the Helmholtz mode. A special feature of this mode is that its eigenfrequency is equal to zero and the eigenfunction is a trivial solution of the eigenvalue equation [11].

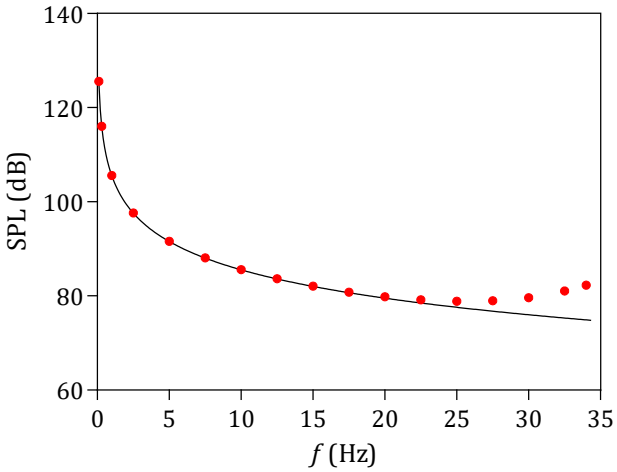

Figure 2. Changes in the SPL with the frequency f: solid line – Eq. (15), red points – results obtained from Eq. (12) based on the mean value of the pressure amplitude on the observation plane.

Calculation data in Fig. 2 illustrate the frequency dependence of SPL in the frequency range from 0.1 Hz to the cut-off frequency f_c. The results obtained from Eq. (15) are marked with a solid line. The red point denote the calculation results received from Eq. (12), but since the pressure amplitude is dependent on the spatial coordinate, the mean value of the pressure amplitude on the observation plane was used in

calculations of SPL. As shown in Fig. 2, the results obtained from Eqs. (12) and (15) are practically the same for frequencies up to 17.5 Hz. Therefore, it can be concluded that in the infrasonic frequency range, the evanescent modes have a negligible effect on the sound field. This impact is much greater for audible frequencies, as evidenced by the increase in discrepancies between the results obtained from Eqs. (12) and (15) for frequencies equal to or greater than 20 Hz.

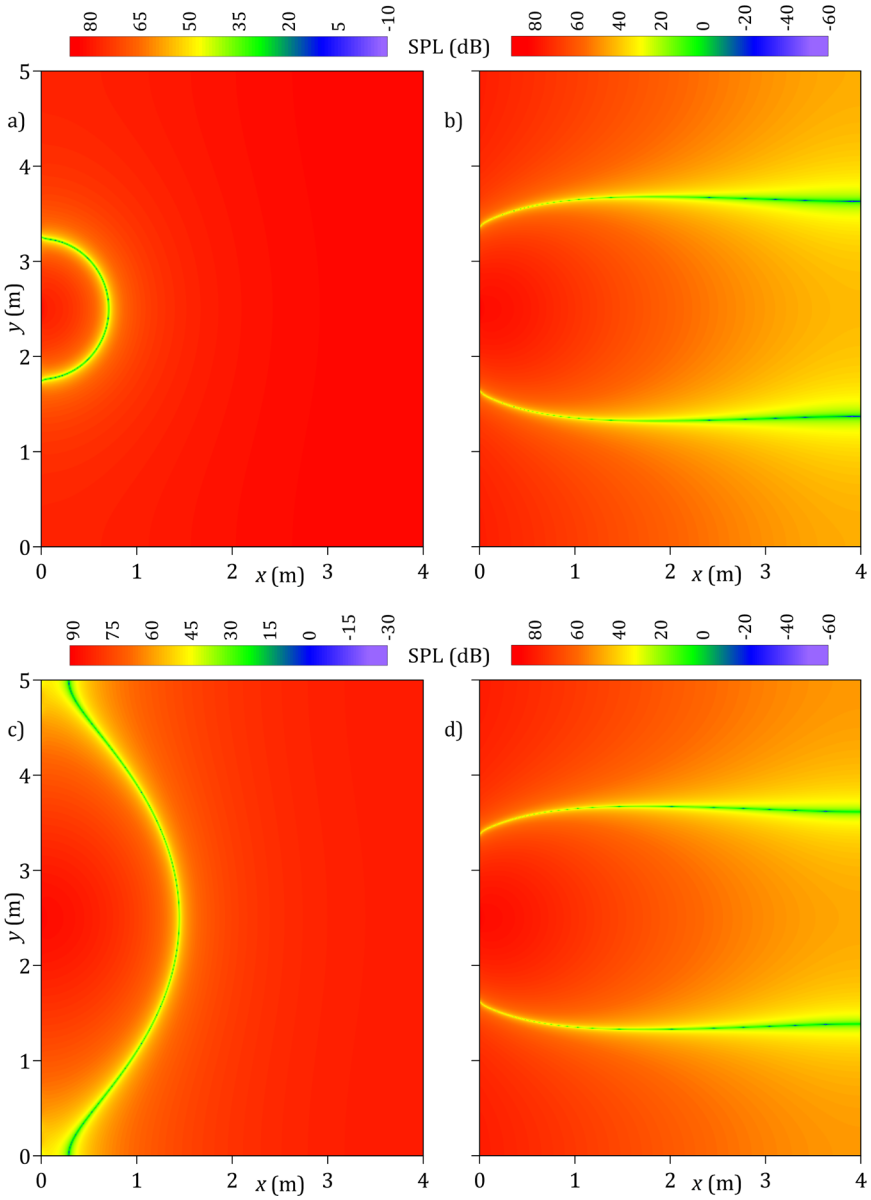

Figure 3. Distribution of SPL on the observation plane at the excitation frequency: a), b) 20 Hz, c), d) 30 Hz, a), c) resultant sound field, b), d) sound field produced by evanescent modes.

The contour maps in Fig. 3a,c show distributions of SPL on the observation plane at the excitation frequency of 20 Hz and 30 Hz. In both cases, large dips in the SPL are observed, which form a continuous curve, the shape of which is different for both frequencies. The contour maps in Fig. 3b,d correspond to the case when the plane wave mode is excluded in Eq. (12), so they show the sound field produced only by evanescent modes. As can be seen, in both cases, distributions of SPL are very similar and this is due to the fact that the same set of evanescent modes co-create the sound field. This proves that the results depicted in Fig. 3a,c are the outcome of the interference of evanescent modes with the plane wave mode having different shape for the considered frequencies. This is confirmed by the calculation results in Fig. 4 showing the distributions of SPL only for the plane wave mode. As seen in Fig. 4a, for the frequency of 20 Hz, the value of SPL changes relatively little in the plane wave mode. Much more large changes in SPL are observed

for the frequency of 30 Hz. They result from a big decrease in the SPL at $x = 1.14$ m, because for this value of x the function $\cos[k(L_x - x)]$ in Eq. (12) equals zero, which means that the component corresponding to the plane wave mode does not contribute to the resultant SPL.

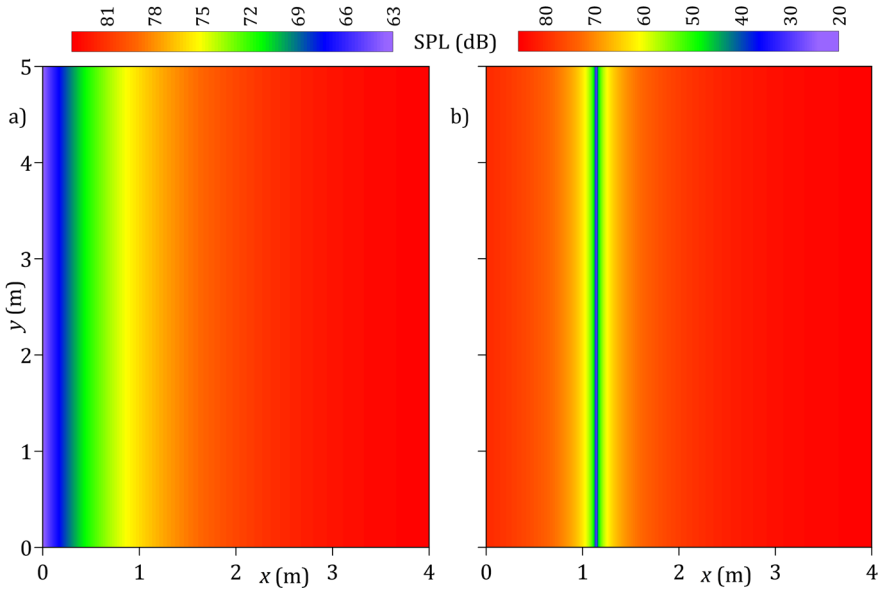

Figure 4. Distribution of SPL on the observation plane for the plane wave mode at the excitation frequency: a) 20 Hz and b) 30 Hz.

In order to explain unusual forms of a sound field at the excitation frequency of 20 Hz and 30 Hz, Fig. 5 shows SPL changes on the section : $0 < x \leq 4$ m, $y = 2$ m, $z = 1.6$ m, for both the plane wave mode (blue line) and evanescent modes (red line). These data indicate that large dips in the SPL observed in Fig. 3a,c occur when the sound associated with the plane wave mode is cancelled by the sound produced by evanescent modes. This means that the sound pressures generated by the plane wave and evanescent modes have the same amplitude but different sign, so the resultant sound pressure changes sign and goes through zero. This is evidenced by the fact that in Fig. 5 the blue and red lines intersect at point corresponding exactly to the large drop in the resultant SPL (black dashed line).

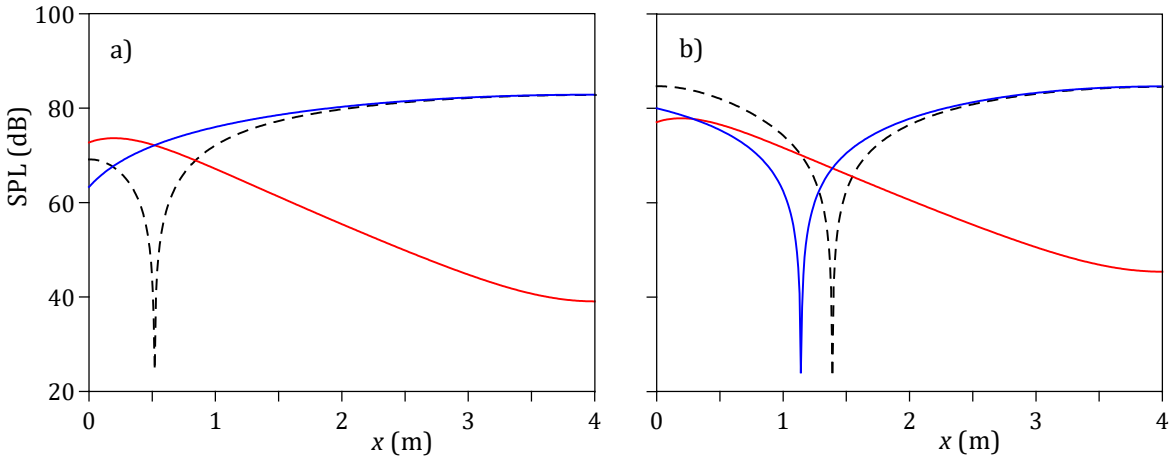

Figure 5. SPL changes on the section: $0 < x \leq 4$ m, $y = 2$ m, $z = 1.6$ m, for the excitation frequency: a) 20 Hz and b) 30 Hz. Blue line – SPL for plane wave mode, red line – SPL for evanescent modes, black dashed line – resultant SPL.

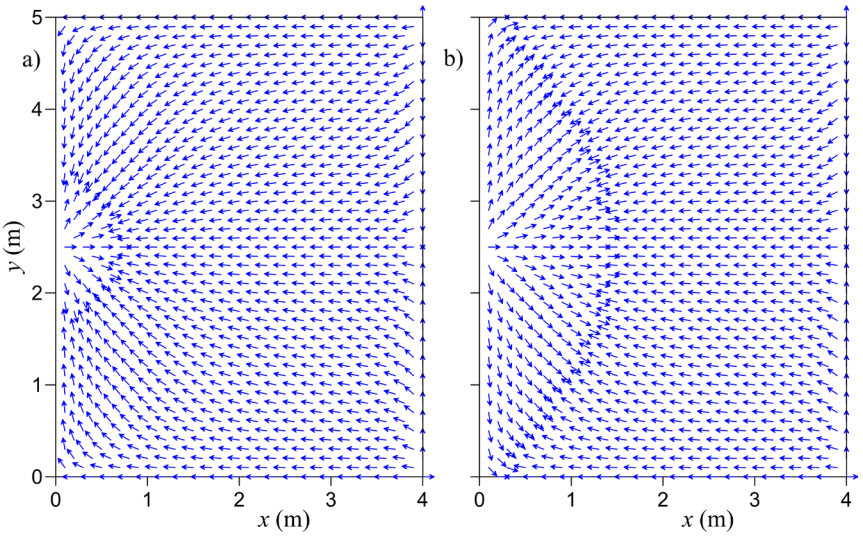

Figure 6. Vector field showing the direction of the reactive sound intensity **Q** on the observation plane at the excitation frequency: a) 20 Hz and b) 30 Hz.

The theoretical results in Sect. 2 show that in the rigid-walled room there is only the reactive sound intensity **Q** representing the imaginary part of the complex sound intensity $\mathbf{I}_c$. Unfortunately, it turned out that the magnitude $|\mathbf{Q}|$ varies in a very wide range, which means that it is very difficult to reproduce the vector **Q** correctly. However, assuming that this magnitude is the same at every point inside the room, it is possible to reconstruct the direction of **Q** on the observation plane. The vector fields obtained in this way are depicted in Fig. 6, which shows the direction of **Q** at the excitation frequency of 20 Hz and 30 Hz. As can be seen from the comparison between Figs. 3a,c and 6, the reactive sound intensity vector is pointed in the direction of decreasing pressure. This regularity is confirmed mathematically by the equation [11]

$$\mathbf{Q}(\mathbf{r}) = -\frac{1}{2\rho\omega} P(\mathbf{r}) \nabla P(\mathbf{r}), \tag{17}$$

which also shows that the vector **Q** is always perpendicular to the surfaces of constant pressure.

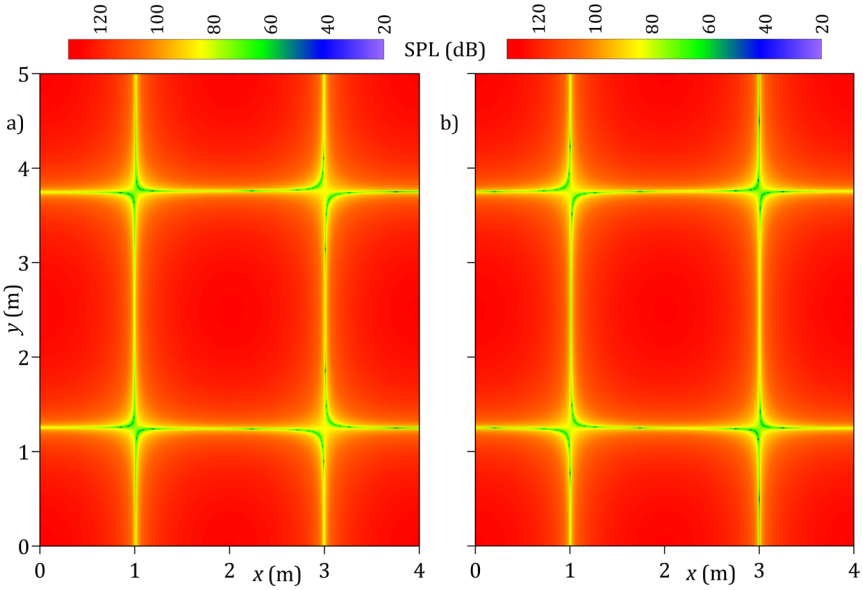

Figure 7. Distribution of SPL on the observation plane at the excitation frequency of 110 Hz, a) resultant sound field, b) sound field produced by cut-on modes.

Above the cut-off frequency f_c, more and more evanescent modes become cut-on modes when the excitation frequency f increases. The number M of cut-on modes up to the frequency f for a rigid-walled rectangular room can be determined from the expression [12]

$$M = \frac{1}{L_y}\left[\frac{\pi V}{6L_y^2}\left(\frac{f}{f_c}\right)^3 + \frac{\pi S}{16L_y}\left(\frac{f}{f_c}\right)^2 + \frac{L}{16}\left(\frac{f}{f_c}\right)\right], \tag{18}$$

where V, as before, is the room volume, $S = 2\left(L_xL_y + L_xL_z + L_yL_z\right)$ is the surface of all room walls and $L = 4\left(L_x + L_y + L_z\right)$ is the sum of lengths of room edges. As follows from Eq. (18), if the frequency is much higher than the cut-off frequency, then the effect of evanescent modes on the sound field is expected to decrease. This is confirmed by calculation results, which demonstrate that above the excitation frequency of 100 Hz, the impact of evanescent modes on the sound field is small, and this is especially noticeable for frequencies equal to or close to resonance frequencies. Such a case is depicted in Fig. 7 because it shows that at the excitation frequency of 110 Hz, which is close to the frequency of the 18th normal acoustic mode, the resultant sound field and the sound field produced by cut-on modes are almost the same.

4. Concluding remarks

This paper was concerned with the theoretical and numerical studies of the sound field generated by a boundary time-harmonic source in rigid-walled rectangular rooms. The analytical model showed that an excited sound field is produced by a finite number of cut-on modes and an infinite number of evanescent modes. The obtained numerical results demonstrated that below the cut-off frequency there is a strong interference between the plane wave mode and evanescent modes, which results in large pressure level drops forming a continuous curve on the observation plane. The shape of this curve was found to be highly dependent on the excitation frequency. Calculation data has shown that these dips occur when the sound associated with the plane wave mode is cancelled by the sound produced by evanescent modes. The influence of evanescent modes on the sound field turned out to be small when the frequency is much higher than the cut-off frequency, and this is especially evident for frequencies equal to or close to resonance frequencies of a room.

Additional information

The author(s) declare: no competing financial interests and that all material taken from other sources (including their own published works) is clearly cited and that appropriate permits are obtained.

References

1. P.M. Morse, K.U. Ingard; Theoretical Acoustics; Princeton University Press, 1987
2. F. Jacobsen, P.M. Juhl; Fundamentals of General Linear Acoustics; John Wiley & Sons Ltd., 2013
3. U. Ingard; On the theory and design of acoustic resonators; J. Acoust. Soc. Am., 1953, 25(6), 1037–1061; DOI: 10.1121/1.1907235
4. A. Selamet, Z.L. Ji; Circular asymmetric Helmholtz resonators; J. Acoust. Soc. Am., 2000, 107(5), 2360–2369; DOI: 10.1121/1.428622
5. J.W. Lee, J.M. Lee, S.H. Kim; Acoustical analysis of multiple cavities connected by necks in series with a consideration of evanescent waves; J. Sound Vib., 2004, 273(3), 515–542; DOI: 10.1016/S0022-460X(03)00508-X
6. M. Meissner; Acoustics of small rectangular rooms: Analytical and numerical determination of reverberation parameters; Appl. Acoust., 2017, 120, 111–119; DOI: 10.1016/j.apacoust.2017.01.020
7. K. Szemela, W. Rdzanek; The influence of an impedance obstacle on the acoustic field inside a rectangular room; J. Vib. Acoust., 2022, 144(2), 021005; DOI: 10.1115/1.4051587
8. M. Meissner; A novel method for determining optimum dimension ratios for small rectangular rooms; Arch. Acoust., 2018, 43(2), 217–225; DOI: 10.24425/122369
9. H. Kuttruff; Room Acoustics, 5th ed.; Spon Press, 2009
10. Wolfram Mathematical Functions; Site. http://functions.wolfram.com/01.09.06.0007.01
11. M. Meissner; Acoustic energy density distribution and sound intensity vector field inside coupled spaces; J. Acoust. Soc. Am., 2012, 132(1), 228–138; DOI: 10.1121/1.4726030
12. M. Meissner; Spectral characteristics and localization of modes in acoustically coupled enclosures; Acta. Acoust. United Acust., 2009, 95(2), 300–305; DOI: 10.3813/AAA.918152